1 **Title:** Chromatin-immunoprecipitation reveals the PnPf2 transcriptional network

2 controlling effector-mediated virulence in a fungal pathogen of wheat.

3

4 **Running title**

5 PnPf2 regulation of virulence

6

7 **Author names and affiliations:**

8 Evan John[1,#,*], Karam B. Singh[1,2], Richard P. Oliver[3], Jessica L. Soyer[4], Jordi Muria-

9 Gonzalez[1], Daniel Soo[1], Silke Jacques[1] and Kar-Chun Tan[1,#]

10 [1]Centre for Crop and Disease Management, Curtin University, Perth, Australia

11 [2]Agriculture and Food, Commonwealth Scientific and Industrial Research

12 Organisation, Perth, Australia

13 [3]School of Biosciences, Nottingham University, Nottingham, United Kingdom

14 [4]Université Paris-Saclay, INRAE, UR BIOGER, 78850, Thiverval-Grignon, France

15

16 *Current address:

17 Institute of Plant and Microbial Biology, Academia Sinica, Taipei 11529, Taiwan

18

19 #Please direct author inquiries to:

20 Evan John - evan.john@curtin.edu.au

21 Kar-Chun Tan – Kar-Chun.Tan@curtin.edu.au

22

23 **Abstract**

24   The regulation of virulence in plant-pathogenic fungi has emerged as a key area

25   of importance underlying host infections. Recent work has highlighted the role of

26   transcription factors (TFs) that mediate the expression of virulence-associated genes.

27   A prominent example is Pf2, a member of the Zn_2Cys_6 family of fungal TFs, where

28   orthologues regulate the expression of genes linked to parasitism in several plant-

29   pathogen lineages. These include PnPf2 which controls effector-gene expression in

30   *Parastagonospora nodorum*, thereby determining the outcome of effector-triggered

31   susceptibility on its host, wheat. PnPf2 is a promising target for disease suppression

32   but the genomic targets, or whether other are regulators involved, remain unknown.

33   This study used chromatin immunoprecipitation (ChIP-seq) and a mutagenesis

34   analysis to investigate these components. Two distinct binding motifs connected to

35   positive gene-regulation were characterised and genes directly targeted by PnPf2

36   were identified. These included genes encoding major effectors and other components

37   associated with the *P. nodorum* pathogenic lifestyle, such as carbohydrate-active

38   enzymes and nutrient assimilators. This supports a direct involvement of PnPf2 in

39   coordinating virulence on wheat. Other TFs were also prominent PnPf2 targets,

40   suggesting it also operates within a transcriptional network. Several TFs were

41   therefore functionally investigated in connection to fungal virulence. Distinct metabolic

42   and developmental roles were evident for the newly characterised PnPro1, PnAda1,

43   PnEbr1 and the carbon-catabolite repressor PnCreA. Overall, the results uphold

44   PnPf2 as the central transcriptional regulator orchestrating genes that contribute to

45   virulence on wheat and provide mechanistic insight into how this occurs.

46

Importance

48   Fungal pathogens cause large crop losses worldwide and consequently much

49   attention has focused on improving host genetic resistance to diseases. These

50   pathogens use effectors, which require coordinated expression at specific stages of

51   the pathogenic lifecycle, to manipulate the host plant metabolism in favour of infection.

52   However, our understanding of the underlying regulatory network in coordination with

53   other genes involved in fungal pathogenicity is lacking. The Pf2 TF orthologues are

54   key players underpinning virulence and effector gene expression in several fungal

55   phytopathogens, including *P. nodorum*. This study provided significant insight into the

56   DNA-binding regulatory mechanisms of *P. nodorum* PnPf2, as well as further evidence

57   that it is central to the coordination of virulence. In the context of crop protection, the

58   Pf2 taxonomic orthologues present opportune targets in major fungal pathogens that

59   can be perturbed to reduce the impact of effector triggered-susceptibility and improve

60   disease resistance.

61

62

63   **Keywords**

64   Transcription factor, virulence, regulation, gene expression, orthologue

65   **Abbreviations**

66   Transcription factor (TF), DNA-binding domain (DBD), chromatin immunoprecipitation

67   (ChIP), carbohydrate-active enzyme (CAZyme), amino acid (a.a), gene ontology (GO)

1. Background

The *Parastagonospora nodorum*-wheat interaction has become a model fungal-plant pathosystem to study the molecular virulence factors underpinning infection. The fungus produces small secreted effector proteins that selectively interact with host-receptors encoded by dominant susceptibility-genes (1, 2). These interactions occur in a gene-for-gene manner that causes 'effector-triggered susceptibility' in the host plant, quantitatively affecting the disease which manifests as septoria nodorum blotch. Several effectors acting in this manner have now been identified and characterised for their role in virulence (3–7). These studies have also described a consistent pattern: the expression of these genes is maximal two to four days after infection and then declines. Furthermore, expression levels can vary by the presence or absence of their matching wheat receptors, as well as by epistasis, whereby one effector gene causes suppression of another (8–10). Yet relatively little is known concerning the mechanisms governing the effector gene regulation. In particular, are there common or distinct regulatory pathways involved? Do these components specifically control effector gene expression, or co-regulate other metabolic and developmental pathways? New knowledge in this area could present suitable targets to suppress for disease control.

Many fungi possess a Zn_2Cys_6 transcription factor (TF) Pf2 that has been associated with the regulation of effector gene expression. One example is the AbPf2 orthologue in *Alternaria brassicicola* that is critical for virulence on *Brassica* spp. (11). Gene deletion of *AbPf2* resulted in the down-regulation of a number of effector like genes, as well as putative cell-wall degrading enzymes. In *P. nodorum*, at least two key effector genes, *ToxA* and *Tox3*, require PnPf2 t be expressed (12). An RNA-seq

4

93   analysis also revealed PnPf2 regulates many more putative effectors, CAZymes,

94   hydrolases/peptidases and nutrient transporters (13). The PtrPf2 orthologue in

95   *Pyrenophora tritici-repentis* controls *ToxA* expression and virulence on wheat, much

96   like for the homologous *ToxA* gene in *P. nodorum* (12). In *Leptosphaeria maculans*,

97   the causal agent of blackleg disease on *Brassica* spp., the LmPf2 orthologue also

98   regulates several effector genes, including *AvrLm4-7, AvrLm6,*

99   *AvrLm10A* and *AvrLm11*, as well as CAZyme expression (14).

100

101   The Pf2 orthologues can be traced across several Ascomycota fungal lineages

102   that include the Dothideomycetes, Leotiomycetes and Soradiomycetes (15). Gene-

103   deletion in the plant pathogens *Botrytis cinerea*, *Fusarium* spp., *Magnaporthe oryzae*

104   and *Zymoseptoria tritici* all suppressed fungal virulence as well as their capacity to

105   utilise alternative carbon sources (16–19). Analogous carbohydrate regulatory roles

106   have been attributed in the saprophytic fungi *Neurospora crassa* and *Trichoderma*

107   *reesei* (20, 21). In *N. crassa*, the putative orthologue Col-26 is a critical component

108   within a signalling-network that responds to glucose availability and promotes the

109   expression of CAZymes for plant cell-wall degradation (22–24). There is a strong

110   association between CAZyme gene content and plant-pathogenic lifestyles (25).

111

112   There are some key factors yet to be established among Pf2 orthologues. Which

113   DNA-regulatory elements are bound? Are Pf2-regulated genes directly targeted or is

114   their expression modulated by indirect factors? Are there other TFs intimately

115   connected with Pf2 regulation of virulence? The research presented here provides

116   such critical insight for PnPf2 in *P. nodorum*, and establishes its direct role in effector

117   expression and CAZyme regulation. A subsequent functional investigation of several

118   connected and directly targeted TFs provides further evidence for the central role held

119   by PnPf2 in the transcriptional network that orchestrates virulence in *P. nodorum*.

120

121   **2.   Results**

122   **2.1.   PnPf2 possesses typical Zn_2Cys_6 TF domains and localises to the**

123   **nucleus.**

124   Conserved domains or distinguishing features were analysed in the 652 amino

125   acid (a.a) PnPf2 protein. The Zn_2Cys_6 DNA binding domain was located N-terminally

126   at a.a 9 to 54 with an overlapping nuclear localisation signal (NLS) (KKGPKGSR; a.a

127   51 to 58) (**Fig. 1A**). A 'fungal TF domain' was identified from a.a 223 to 294 within a

128   conserved 'middle homology region' (a.a 104 to 320). These features are frequently

129   observed in Zn_2Cys_6 TFs and have been linked to the modulation of TF activity (26,

130   27, 15). A structurally disordered domain, typically associated with post-translational

131   modifications and intermolecular interactions (28), was also identified at the C-

132   terminus of PnPf2. Together, these features suggested that PnPf2 possesses the

133   typical functional domains underpinning DNA-binding Zn_2Cys_6 TF activity (26). Nuclear

134   localisation of the C-terminally tagged PnPf2-GFP fusion protein was also observed

135   (**Fig. 1B**). Along with the functional domains identified, this supported DNA-binding

136   regulatory activity by PnPf2.

137

138   **Fig. 1 HERE**

139

2.2.   Two direct PnPf2 target motifs are associated with gene-regulation

A chromatin immunoprecipitation (ChIP) analysis was used to define PnPf2-DNA binding *in situ*. The *Pf2-HA* (native promoter) and *Pf2-HA_OE* (overexpression promoter) strains expressing the 3x haemagglutinin (HA) tagged PnPf2-HA fusion protein retained PnPf2 function, in contrast to a *pf2-HA_KO* deletion control (**Text S1**). A ChIP-seq analysis was therefore undertaken using the *Pf2-HA* and *Pf2-HA_OE* strains to identify 'summits' within enriched 'peak' regions. Summits corresponded to the best estimate of PnPf2-DNA binding loci within the peaks (29). The *Pf2-HA* and *Pf2-HA_OE* samples provided complementary datasets; the overexpression mutant to compensate for lower *PnPf2* expression under culture conditions (13, 30) and broaden the DNA interactions captured. A total of 997 summits were obtained from the *Pf2-HA* dataset and 2196 from *Pf2-HA_OE*, corresponding to 740 and 1588 peak regions respectively. There were 588 shared peaks identified between the samples (**File S1**), indicating strong overlap between the predicted PnPf2-targeted regions. The *Pf2-HA_OE* dataset broadened the scope of putative binding sites. A quantitative PCR (qPCR) analysis was then undertaken on independently prepared ChIP DNA, comparing the *Pf2-HA* and *Pf2-HA_OE* samples to the *pf2-HA_KO* control. Fold-enrichment values relative to *pf2-HA_KO* strongly correlated with ChIP-seq summit -Log_{10}(Q-values), a proxy measure for PnPf2-DNA binding affinity, in both the *Pf2-HA* (P < 0.01 with Pearson's r = 0.77) and *Pf2-HA_OE* (P < 0.01 with Pearson's r = 0.74) datasets (**Text S1**). The high reproducibility across separate methodologies provided confidence in the robustness of ChIP-seq summit calls.

Text S1 HERE

165   **File S1 HERE**

166

167   Previous RNA-seq differential-expression analyses had identified an enriched

168 consensus motif (5'-WMGGVCCGAA-3') in the promoter regions of both AbPf2 and

169 PnPf2-regulated genes (11, 13). Despite harbouring the typical 'CGG' Zn_2Cys_6 binding

170 triplet (26), an interaction with PnPf2 was not observed in a heterologous system,

171 indicating regulatory cofactors may be required (31, 13). A search for DNA-regulatory

172 elements that interact with PnPf2 from the ChIP-seq dataset identified two enriched

173 motifs in the merged *Pf2-HA* and *Pf2-HA_OE* peak regions (**Fig. 2A**). The first motif

174 designated as M1 (5'-RWMGGVCCGA-3') closely matches the consensus motif from

175 AbPf2 and PnPf2-regulated gene promoters (11, 13). The second motif designated as

176 M2 (5'-CGGCSBBWYYKCGGC-3') is novel for PnPf2, encompassing two copies of

177 the canonical 'CGG' Zn_2Cys_6 binding triplets (26), separated by eight nucleotides.

178 Interestingly, M2 matches the AmyR regulatory response element that was modelled

179 in *A. nidulans* (32). Both M1 and M2 are close to the ChIP-seq summits for the *Pf2-*

180 *HA* and *Pf2-HA_OE* datasets (**Fig. 2B**), suggesting they accurately reflected DNA-

181 binding loci.

182

183   The previous RNA-seq analysis had defined genes positively or negatively-

184 regulated by PnPf2 from their expression changes in the *PnPf2*-deletion mutant *pf2ko*

185 relative to wildtype SN15 (13). These gene sets include the *in vitro* culture conditions

186 that were replicated here for ChIP to maximise TF-DNA yields, as well as an early

187 fungal infection stage *in planta* (72 hrs). Instances of M1 and M2 were then identified

188 across the promoters of the positive (i.e. *pf2ko*-down) and negative (*pf2ko*-up) PnPf2-

189 regulated gene sets (**File S2**). Both M1 and M2 were significantly enriched in the

190   positively-regulated gene promoter set only (**Fig. 2A**). This indicates both motifs

191   correspond to cis-regulatory elements that induce, rather than repress, gene

192   expression.

193

194   A novel approach here sought to detect specifically the PnPf2-motif

195   interactions. This utilised a *dTomato* reporter gene fused to the promoter of

196   SNOG_15417. The promoter was chosen to encompass a ChIP-seq peak region with

197   both the M1 and M2 motifs for a gene that is positively-regulated by PnPf2 (**Fig. 2C**;

198   **File S2**). Integration of the construct at a predefined genomic locus in the SN15

199   background permitted evaluation of the reporter-gene expression in the resultant strain

200   (*p15417_M1M2*) in comparison with strains where the CGG triplets in M1 and/or M2

201   had been substituted (*p15417_m1M2*, *p15417_M1m2* and *p15417_m1m2*).

202   Significantly reduced expression was observed in the strains where M1 had been

203   mutated, indicating that it is a functionally important and direct PnPf2 target in the

204   SNOG_15417 promoter (**Fig. 2C**). No significant expression change was detected

205   where only the M2 motif was mutated.

206

207   **Fig. 2 HERE**

208

209 **2.3. PnPf2 directly targets genes associated with the pathogenic**

210 **lifestyle of *P. nodorum***

211 Genes with a ChIP-seq summit in their promoter region, considered a putative

212 PnPf2 target, were cross-referenced with the *pf2ko* RNA-seq data analysis (**File S2**).

213 There were 1286 targets identified from either ChIP-seq dataset, 484 of which were

214 considered 'high-confidence' with a promoter summit in both *Pf2-HA* and *Pf2-HA_OE*

215 (**Fig. 3A**). Of the 484 direct targets, 72 genes were positively-regulated in contrast to

216 6 negatively-regulated genes under the same *in vitro* conditions used for ChIP-seq.

217 This indicates PnPf2 functions mainly as a positive regulator of gene expression.

218 When expanded to also encompass PnPf2-regulated genes *in planta*, 93 were

219 positively while 27 were negatively-regulated genes (**Fig. 3B**). Differential expression

220 was not detected in the pf2ko mutant for 364 genes. This suggests other regulatory

221 factors play a considerable role in their expression.

222

223 **File S2 HERE**

224

225 The characterised effector genes present in *P. nodorum* SN15, *ToxA, Tox1,*

226 *Tox3* and *Tox267* (7), plus 29 other effector-like genes whose expression was altered

227 in the *pf2ko* mutant, were assessed for evidence of direct regulation by PnPf2. Two

228 distinct ChIP-seq summits were identified in the bi-directional *Tox3* promoter (**Fig. S1**).

229 Both the upstream gene (i.e. SNOG_08982, encoding a protein disulphide-isomerase)

230 and downstream gene (*Tox3*) are positively regulated by PnPf2. A ChIP-seq summit

231 was also identified in the *Tox1* promoter, but only from the *Pf2-HA_OE* dataset (**Fig.**

232 **S1**). Unlike Tox3, Tox1 necrosis-inducing activity is still detected in the *pf2ko*

233 background (12), indicating the summit may represent a weak enhancer element. The

234   *ToxA* gene is only expressed during infection but in a PnPf2-dependent manner. A

235   weak promoter summit was observed despite multiple instances of the M1 motif,

236   suggesting another factor(s) is required to facilitate PnPf2-DNA binding that was

237   absent under the ChIP-seq experimental conditions. No distinct PnPf2 summit was

238   observed in the promoter of *Tox267*, whose expression is not significantly altered in

239   the *pf2ko* mutant, although two instances of M1 were identified >1000 bp upstream

240   (**Fig. S1**). In total, 11 of the 29 PnPf2-regulated effector-like genes showed evidence

241   of direct PnPf2-promoter binding through ChIP-seq summits (**Table S1-A**).

242

243   **Fig. S1 HERE**

244

245   A gene-ontology (GO) enrichment and network analysis was then carried out

246   to identify major functional gene classes that are directly regulated by PnPf2. Five

247   distinct groups representing TFs, redox molecules, CAZymes, cell-signalling

248   molecules and nutrient transporters were significantly enriched among the GO

249   networks (**Fig. 3C-D**). The enrichment of CAZymes, redox molecules and nutrient

250   transporters is consistent with enriched functional GO classes that were observed for

251   the *pf2ko* differentially expressed genes (13). In contrast, the TFs and cell-signalling

252   molecules were not enriched, indicating they could be tightly controlled by redundant

253   pathways in addition to PnPf2. Nevertheless, it was striking that TF genes were

254   particularly enriched in the high-confidence set of 484 targets (**Fig. 3C-D**). They made

255   up 9.1% of these genes in contrast to 3.5% of the total genes annotated for SN15.

256   Five TFs were directly targeted and positively regulated, providing a direct connection

257   with PnPf2 in the regulation of virulence (**Table S1-B**).

258

259   **Fig. 3 HERE**

260

261   **Table S1 HERE**

262

263 **2.4. PnPf2 is the central transcriptional regulator of host-specific**

264 **virulence**

265 The identification of TFs as major PnPf2 targets prompted a functional

266 exploration of other TFs with a putative intermediate role in regulating virulence. Three

267 directly-regulated TF genes were therefore targeted for deletion where orthologues

268 had virulence-associated roles (**Table 1**). These included SNOG_03490 (*PnPro1*),

269 SNOG_04486 (*PnAda1*) and SNOG_08237. Two additional TF-encoding genes were

270 simultaneously investigated. This included SNOG_08565, identified in the PnPf2

271 lineage of fungal TFs (15) suggesting a possible common evolutionary origin. It also

272 included SNOG_03067 (*PnEbr1*), which is co-expressed with *PnPf2, ToxA*, *Tox1* and

273 *Tox3* high during early infection (**Fig. S2**), suggesting a similarly important role in

274 disease.

275

276 **Fig. S2 HERE**

277

278 Gene deletion strains for the five TFs were phenotypically characterised in

279 comparison to wildtype SN15 and *pf2ko*. The *pro1_KO*, *ada1_KO* and *ebr1_KO*

280 deletion mutants presented distinct phenotypic abnormalities (**Fig. 4**). The *pro1_KO*

281 mutants were abolished in their ability to form pycnidia and sporulate both during

282 infection and on nutrient-rich agar. However, vegetative growth was expansive in both

283 conditions (**Fig. 4A-B**), suggesting PnPro1 acts to suppress hyphal development.

284 Although *PnPro1* is positively-regulated by PnPf2, there was no distinct phenotypic

285 overlap with the *pf2ko* mutant. The *ada1_KO* mutant was significantly reduced in

286 virulence on detached leaves (**Fig. 4A-B**). Dark brown discolouration at the site of

287 infection suggested a hypersensitive response had contained the infection. We also

14

288   observed an increased susceptibility to oxidative (H_2O_2) stress for *ada1_KO* mutants

289   similar to *pf2ko*. Furthermore, sporulation was reduced in *ada1_KO* relative to SN15

290   (**Fig. 4C-E**). The *ebr1_KO* mutants exhibited vegetative growth defects with an uneven

291   growth perimeter around the colony edges coinciding with perturbed virulence (**Fig.**

292   **4A-B**). Similar hyphal-branching defects were described following deletion of *PnEbr1*

293   orthologues in *Fusarium* spp. (33, 34). Interestingly, the *ebr1_KO* mutants were also

294   susceptible to H_2O_2 stress at a level comparable to *pf2ko* and *ada1_KO*. Furthermore,

295   pycnidia were abnormally developed, although still viable for the production of conidia,

296   but were not detected on infected leaves (**Fig. 4C-D**). We did not observe

297   morphological or virulence defects for the *08237_KO* or *08565_KO* mutants (**Text S2**)

298   which were not investigated in further detail.

299

300   **Fig. 4 HERE**

301

302   During the course of this study the carbon-catabolite repressor (CCR) element

303   was modelled as the binding site for the Cre-1 TF that suppresses CAZyme expression

304   in *N. crassa* (22). We noted this was near identical to a motif (5'-RTSYGGGGWA-3')

305   that is also enriched in PnPf2-regulated gene promoters (13) but not identified from

306   the ChIP-seq peaks. Since Cre-1 orthologues are conserved CCR regulators in

307   filamentous fungi (35, 36), and since the CCR element is also enriched in PnPf2

308   regulated gene promoters, a putative Cre-1 orthologue (PnCreA) was investigated in

309   *P. nodorum* to identify common regulatory pathways with PnPf2. Both *PnCreA*

310   overexpression and gene-deletion mutants (*CreA_OE* and *creA_KO*) were created

311   and then investigated alongside *pf2ko* and a *PnPf2* overexpression mutant (*Pf2_OE*).

312   Despite clear phenotypic-growth abnormalities (**Fig. 5**), neither the *CreA_OE* nor

313   *creA_KO* mutants exhibited virulence defects on wheat leaves (**Text S2**). The

314   *creA_KO* strain was enhanced in starch utilisation (**Fig. 5**), an indicator substrate for

315   CCR activity (37). In contrast, there was a moderate reduction of *pf2ko* to utilise starch,

316   similar to observations in other fungal *PnPf2*-orthologue mutants (17, 19, 21). These

317   results support contrasting roles between PnCreA and PnPf2 for the regulation of

318   some CAZyme-related genes.

319

320   **Fig. 5 HERE**

321

322   **Text S2 HERE**

323

324   **Table 1 HERE**

325

326   **3.   Discussion**

327   Prior to this research, PnPf2 had been identified as an important regulator of *P.*

328   *nodorum* virulence on wheat (12, 13), but important details and mechanistic insights

329   were missing. We sought to take further steps and establish the DNA-binding elements

330   targeted by PnPf2 and identify genes that were directly under its direct regulation. Two

331   distinct regulatory motifs M1 and M2 were identified and linked to positive gene-

332   regulation by PnPf2. M1 was strikingly similar to an enriched sequence in AbPf2

333   positively-regulated gene promoters (11), possibly representing a conserved Pf2

334   binding mechanism. It will be pertinent to explore this motif as a regulatory target for

335   other fungal Pf2 orthologues (11–14, 16–21). Interestingly, the M2 motif matches the

336   extensively characterised AmyR regulatory-response element in *A. nidulans* (38, 32).

337   Polysaccharide metabolism has long been established as a regulatory function for

338   AmyR (39, 40). Therefore, some shared regulatory pathways likely exist with Pf2

339   orthologues given the evidence for at least one conserved binding mechanism.

340   However, there are major a.a polymorphisms between AmyR and Pf2 orthologues at

341   the Zn_2Cys_6 DNA-binding domain (15) and M1 has not been reported as an AmyR

342   target despite extensive motif investigation (38, 32). It is therefore conceivable that M1

343   is a regulatory binding element unique to Pf2 orthologues and therefore useful to

344   identify putative direct targets such as *ToxA* in *P. nodorum.*

345

346   The ChIP-seq PnPf2-DNA binding dataset also facilitated the identification of

347   *P. nodorum* genes under direct PnPf2 regulation. Among these genes is the *Tox3*

348   effector and the adjacent gene, SNOG_08982, encoding a protein disulphide

349   isomerase. This class of protein catalyses cysteine-cysteine bond formation which has

350   been connected to fungal effector protein production (41). Therefore, it would be worth

351   exploring any involvement of SNOG_08982 in the post-translational modification of

352   Tox3 and other effectors. PnPf2 binding was also detected in the *Tox1* promoter. A

353   partial reduction in *Tox1* expression was reported in the *pf2ko* mutant (13), indicating

354   PnPf2 is not essential but enhances expression under favourable conditions. *ToxA* is

355   only expressed *in planta,* but is PnPf2 dependent (12). Despite multiple instances

356   matching the M1 motif, there was little evidence for PnPf2-*ToxA* promoter binding,

357   suggesting chromatin inaccessibility or the absence of essential binding-cofactors

358   under the ChIP culture conditions. Direct PnPf2 regulation of *Tox267* was not evident.

359   The other recently-cloned effector gene *Tox5* is not present in the SN15 isolate used

360   in this study, but is homologous to *Tox3* may be under PnPf2 control (6). Nevertheless,

361   several other effector-like genes were identified as direct PnPf2 targets (**Table S1-A**).

362   Importantly this analysis provided strong evidence that PnPf2 is a key direct-regulator

363   of effectors, the major *P. nodorum* virulence factors in the lifestyle of this pathogen.

364

365   Evidence for regulation of effector expression has been reported for another *P.*

366   *nodorum* TF PnCon7 (42), yet its apparent requirement for fungal viability renders it

367   difficult to investigate a precise functional role. Here, several novel TFs were

368   functionally investigated based on their connection to PnPf2 (**Table 1**). We did not

369   observe any change in the necrosis-inducing activity on wheat of fungal culture filtrates

370   derived from the respective mutants. However, developmental virulence roles,

371   including oxidative stress tolerance and hyphal development, were identified for *P.*

372   *nodorum* PnAda1 and PnEbr1. It is possible that the direct regulation of PnAda1 by

373   PnPf2 contributes to the susceptibility to oxidative stress also identified in the *pf2ko*

374   mutant. The PnCreA orthologue of *N. crassa* Cre-1 was also investigated, following

375   the striking observation that the *N. crassa* Cre-1 CCR element (5′-TSYGGGG-3') was

376   enriched in PnPf2-regulated gene promoters (13). Furthermore, Cre-1 and the PnPf2

377   orthologue Col-26 are both key components of a transcriptional network controlling

378   CAZyme production in *N. crassa* (22–24, 43). Here, the *creA_KO* strain displayed an

379   enhanced capacity to utilise starch, which was moderately impaired in the *pf2ko*

380   mutant (**Fig. 5**). This indicates PnCreA and PnPf2 shared a similar function to the

381   respective *N. crassa* orthologues (21). Surprisingly however, despite vegetative

382   growth abnormalities on agar, there was no distinct change in the virulence profile of

383   either the *creA_KO* or *CreA_OE* mutants (**Text S2**). We also failed to detect the CCR

384   element in the promoters of *ToxA*, *Tox1*, *Tox3* or *Tox267* (**File S2**). This suggests that

385   the regulation of host-specific virulence factors critical for *P. nodorum* infection are not

386   subject to CCR by PnCreA.

387

388   This investigation, along with previous TF studies in *P. nodorum* (44, 45, 12,

389   42), indicate PnPf2 is central to the transcriptional-regulatory network controlling

390   virulence, for which a tentative model is proposed (**Fig. 6**). Having expanded our

391   understanding, it also raised some key questions. For many genes directly targeted

392   by PnPf2, differential expression in *pf2ko* has not been observed (364 of 484 high-

393   confidence targets). Such discrepancies are also reported in ChIP-seq experiments

394   on filamentous fungi (**Table S2**). One aspect to consider is that functional TF binding

395   requires specific cofactors/coregulators before gene expression is eventually

396   modulated (46, 47). Furthermore, TF-DNA interactions can be redundant or non-

397   functional (48–50). It is therefore plausible that many binding sites are transiently

398   occupied by PnPf2 in this manner, acting as a biological sink. A change in the

399   epigenetic landscape, for example during growth *in planta*, could open up genomic

400   regions for which PnPf2 exhibits a high affinity and then actively binds. Performing

401   PnPf2 ChIP during early infection will likely prove highly useful in this regard if sufficient

402   fungal material can be obtained. ChIP-seq targeting histone marks specific for

403   euchromatin or heterochromatin under infection conditions, or methylation-sensitive

404   sequencing are alternatives to provide insight into the genome accessibility of PnPf2

405   (14, 51–53). The identification of both the M1 and M2 motifs carrying alternatively

406   oriented 'CGG' triplets, typical of Zn_2Cys_6 monomers (26), was suggestive of PnPf2

407   dimerisation with other Zn_2Cys_6 TFs. However, deletion of the putative ancestral PnPf2

408   homologue SNOG_08565 did not provide any phenotypic response that would

409   indicate a connection. Therefore, future investigations will do well to explore these

410   interactions, for example through co-immunoprecipitation/affinity purification analysis

411   or a yeast-2-hybrid screen, to delineate PnPf2-DNA binding mechanisms. Functional

412   investigation of the PnPf2 'middle homology region' and C-terminal disordered region

413   may also provide insight into the upstream signalling pathways that activate or repress

414   PnPf2 activity through these domains.

415

416   To conclude, this study presents direct evidence of DNA binding in a Pf2

417   orthologue, where virulence-regulatory functions are consistently observed in

418   phytopathogenic fungi. In *P. nodorum*, PnPf2 is central to the transcriptional regulation

419   of virulence and directly controls effector expression. The current research on PnPf2

420   now provides a platform to further investigate its signalling pathways and molecular

421   interactions that could be inhibited for targeted disease control.

422

423   **Fig. 6 HERE**

424

425   **Table S2 HERE**

4. Materials and methods

4.1. Annotations and PnPf2 domain analysis

426 **4. Materials and methods**

427 **4.1. Annotations and PnPf2 domain analysis**

428 The *P. nodorum* annotated genome for the reference isolate SN15 (54) was

429 used consistent with annotations in the previous RNA-seq analysis (13). The PnPf2

430 polypeptide sequence was submitted to Interproscan (Release 82.0) for Interpro and

431 Conserved-Domain-Database domain identification (55). NLStradamus was used to

432 predict the nuclear localisation signal (56). The disordered region was predicted using

433 IUPRED2A (28).

434

435 **4.2. Generation and assessment of fungal mutants**

436 The molecular cloning stages, the constructs generated and diagrammatic

437 overview of the final transformed *P. nodorum* mutants generated in this study are

438 detailed in **Text S3**. The respective primers designed for fragment amplification and/or

439 screening are outlined in **File S3**. Fungal mutants used in this study are summarised

440 in **Table 2**. Their phenotypic and gene-expression analysis procedures are also

441 described in **Text S3.**

442

443 **Table 2. HERE**

444

445 **Text S3 HERE**

446

447 **File S3 HERE**

448

21

4.3. Chromatin immunoprecipitation sample preparation

449

450   The *Pf2-HA*, *Pf2-HA_OE* and *pf2-HA_KO* strains were prepared following 3

451   days standardised growth in 100 mL Fries3 liquid medium (**Text S3**). Prior to

452   harvesting, a 5 mL crosslinking solution (10% w/v formaldehyde, 20 mM EDTA and 2

453   mM PMSF dissolved in 50 mM NaOH) was added with continuous shaking at 100 rpm

454   for 10 min. To this, 5 mL quenching solution (1.25 M glycine) was added before

455   another 10 min shaking. Whole protein extracts were then obtained as described (**Text**

456   **S3**) with modifications for ChIP. The 50 mM Tris was replaced with 50 mM HEPES in

457   the lysis buffer while gentle rotation of the resuspended fungal material was replaced

458   by eight rounds of sonication using a Bandelin (Berlin, Germany)

459   UW3100+SH70+MS73 tip sonicator to fragment the fungal DNA (set at 15 sec on/off

460   with 60% amp and 0.8 duty cycle). Samples were held in an ice block during

461   sonication. The supernatant was then retrieved from two rounds of centrifugation

462   (5000 g, 4 °C for 5 min). A 100 μL aliquot of the supernatant was reserved as an 'input

463   control' against which ChIP samples were to be normalised. A 1000 μL aliquot was

464   then precleared for immunoprecipitation by gently rotating with 20 μL Protein A

465   dynabeads (10001D - Thermofisher, Waltham, Massachusetts) for 1 hr at 4 °C. The

466   supernatant was then retrieved and incubated with 2.5 μg anti-HA polyclonal antibody

467   (71-5500 - Thermofisher) for 16 hrs at 4 °C. Another 20 μL Protein A dynabeads were

468   then added and gently rotated for 2 hrs at 4 °C. The dynabeads were then retrieved

469   and washed twice with 1mL ice-cold lysis buffer, once with high-salt buffer (lysis buffer

470   + 500 mM NaCl), once with LiCl buffer (250 mM LiCl, 10 mM Tris-HCl, 1 mM EDTA,

471   0.5% NP40 and 0.5% NaDOC) and once with TE buffer (10 mM Tris-HCl, 1 mM EDTA,

472   pH 8). Samples were then incubated in a shaking incubator for 10 min (300 rpm, 65

473   °C) with 200 μL elution buffer (0.1 M NaHCO$_3$, 10 mM EDTA and 1% SDS) before

474   transferring the supernatant to a fresh tube. The input control was also supplemented

475   with 100µL elution buffer at this stage and 8 µL NaCl solution (5 M) was added to both

476   samples before de-crosslinking for 16 hrs at 65 °C. To these samples, 200 µL of H_2O

477   and 100 µg RNAse A (QIAGEN, Hilden, Germany) were added before incubating for

478   1 hr at 65 °C. Ten µg Proteinase K (Sigma-Aldrich, St. Louis, Missouri) was then added

479   before incubating a further 1 hr at 50 °C.

480

481   For ChIP-qPCR, DNA (for both the *Pf2-HA*, *Pf2-HA_OE* and *pf2-HA_KO* ChIP

482   and input control samples) was recovered from Proteinase K treated samples using

483   the GenElute PCR purification kit (Sigma-Aldrich).

484

485   For ChIP-seq analysis, DNA (for both *Pf2-HA* and *Pf2-HA_OE* ChIP and input

486   control samples) was purified from the Proteinase K treated samples by mixing in 1

487   volume (400 µL) of phenol:chloroform. This was centrifuged for 5 min at 16000 g and

488   the aqueous phase retrieved. To this, 400µL chloroform was added, mixed and spun

489   (16000 g 5 min) before 350 µL of the aqueous phase was transferred to a fresh tube.

490   35 µL sodium acetate (3 M, pH 5.2) was added with 1 µL of glycogen (20mg/mL).

491   Samples were mixed by inversion and 1 mL 100% ethanol added before precipitation

492   at -80 °C for 1-2 hrs. Pellets were retrieved by spinning 16000 g for 10 min at 4 °C,

493   then washed in 1 ml of ice-cold 70% ethanol before drying and resuspension in 30 µL

494   Tris-Cl (10 mM).

495

496   Two independent DNA preparations for each sample (i.e. the ChIP and input

497   samples for both *Pf2-HA* and *Pf2-HA_OE*), beginning with the fungal growth stage in

498   Fries3 broth, were pooled to ensure sufficient DNA was obtained for generating ChIP-

499   seq libraries. The pooled DNA was measured using a Tapestation system (Agilent,

500   Santa Clara, California). 10 ng of each sample was processed using the TruSeq ChIP

501   Library Preparation Kit (Illumina, San Diego, California). Libraries were size-selected

502   (100-300 bp) and split across four separate lanes for sequencing in a NextSeq 500

503   sequencer (Illumina) to obtain 2 x 75 bp paired-end reads (Australian Genome

504   Research Facility, Melbourne, Australia).

505

506   ### 4.4.   ChIP-seq analysis

507   An overview of the following data analysis pipeline from QC of raw reads

508   through to genome mapping, ChIP-seq peak/summit calling, target gene prediction,

509   ChIP-qPCR validation, GO enrichment analysis and motif position-weight-matrix

510   (PWM) modelling **Text S1**.

511

512   ### 4.4.1.   Raw read filtering, mapping and peak/summit calling

513   Raw reads were checked using FASTQC (Version 0.11.9) (57) and the adapter

514   sequences were trimmed using Cutadapt (Version 1.15) along with nucleotides where

515   the Illumina quality scores were below 30 (58). Optical duplicates were then removed

516   using the 'dedupe' option in Clumpify (version 1.15) from the BBTools package (59).

517   Reads were subsequently mapped to the SN15 genome (54) using BWA-MEM (60).

518   Reads mapping to a single locus as the best match (primary alignments) were retained

519   for downstream analysis and the datasets from sample libraries originally split across

520   the NextSeq lanes were merged using SAMtools (Version 1.10) to produce the final

521   mapped-read datasets (61). MACS (Version 2.2.7.1) was used for calling enriched

522   regions (i.e. peaks) and summits (highest nucleotide point or points within peak

523   regions) from ChIP sample reads relative to the input samples (for *Pf2-HA* and *Pf2-*

524   *HA_OE*). A Q-value peak enrichment threshold of 0.01 was used and the BAMPE

525   option utilised to assess read depth from cognate pairs (62, 63). Paired read lengths

526   from the cognate pairs were assessed using Deeptools 'bamPEFragmentSize'

527   (Version 3.3.0) to verify they corresponded to 100-300 bp size selected fragments

528   (64).

529

530   ### 4.4.2.   Modelling binding-site motifs

531   The overlapping peak regions identified from the *Pf2-HA* and *Pf2-HA_OE*

532   samples were merged using MAnorm (65) to create a consensus set of enriched peak

533   regions containing the putative PnPf2 binding sites. From this set, overrepresented

534   PWMs up to 20 bp long were modelled with MEME (version 5.1.1) (66, 67). For the

535   resulting PWMs, 500 bp genomic regions centred at ChIP-seq summits were extracted

536   and analysed using CentriMo (Version 5.1.1) to verify that the motif instances were

537   also centred at the respective summits for both the *Pf2-HA* and *Pf2-HA_OE* samples

538   (68). Gene promoters (spanning annotated transcription start sites to the nearest

539   upstream gene feature or 1500 bp) with ≥ 1 occurrence of each motif were determined

540   using FIMO (69). These were cross-referenced with the differentially expressed genes

541   (i.e. expressed significantly up or down in *pf2ko* relative to SN15) defined in a previous

542   RNA-seq analysis (13). Fisher's exact test with Bonferroni corrected P-values (70) was

543   used to identify *pf2ko* differentially expressed gene-promoter sets significantly

544   enriched (P_{adj} < 0.01) for the respective motifs vs the background rate in SN15.

545

546   ### 4.4.3.   PnPf2 target gene-promoter analysis

547   Genes targeted by PnPf2 were determined based on the proximity of summits

548   to annotated genes, which were identified using ChIPseeker (Version 1.24.0) (71).

549   Genes with ≥1 summit falling within their promoter region from the *Pf2-HA* or *Pf2-*

550   *HA_OE* datasets were considered PnPf2 targets. High-confidence PnPf2 targets

551   corresponded to genes with a promoter summit in *Pf2-HA* and *Pf2-HA_OE*. ChIP-

552   qPCR was then undertaken to verify that the ChIP-seq peak regions in *Pf2-HA* and

553   *Pf2-HA_OE* would also correlate with quantitative enrichment against the *pf2-HA_KO*

554   control strain. Quantitative PCR primer pairs (**File S3**) were designed to flank ChIP-

555   seq summits in a selection of gene promoters (*ToxA*, *Tox1*, *Tox3*, SNOG_03901,

556   SNOG_04486, SNOG_12958, SNOG_15417, SNOG_15429, SNOG_16438,

557   SNOG_20100 and SNOG_30077) and a selection of non-summit control regions (*Act1*

558   and SNOG_15429 coding sequences and the TrpC terminator). The 'input %' values

559   were calculated for each sample using the method described previously (72) and used

560   to calculate fold-differences (normalised to *Act1*) for *Pf2-HA* and *Pf2-HA_OE* relative

561   to the *pf2-HA_KO* control for comparison with the *Pf2-HA* and *Pf2-HA_OE* -Log$_{10}$(Q-

562   values) at the respective ChIP-seq summit loci. Pearson's correlation coefficient was

563   calculated for the ChIP-qPCR fold-difference and ChIP-seq -Log$_{10}$(Q-values) at the

564   respective loci and used as the test statistic to assess whether the association was

565   significant (SPSS version 27.0).

566

567   The PnPf2 target genes were cross-referenced with the *pf2ko* expression

568   patterns (expressed significantly up or down in *pf2ko*) defined previously (13) to link

569   direct binding with the modulation of gene expression. The SN15 effector-like genes

570   annotated previously (13) were compiled among the PnPf2 targets. Annotated

571   homologues were identified from the corresponding records in UniProt (release

572   2020_05) (73). Both the high-confidence and total PnPf2 target-gene sets were then

573   used for GO enrichment/network analysis using the SN15 GO annotations defined

574   previously (13). The 'enricher' function in the Clusterprofiler package (Version 3.16.0)

575   (74) was invoked to identify the overrepresented GO classes (P < 0.01) in PnPf2

576   targets.

577

578   **4.5.   Data availability statement**

579   The ChIP-seq reads are available under BioProject ID: PRJNA824526,

580   corresponding to BioSamples SAMN27406642 (*Pf2-HA* strain) and SAMN27406643

581   (*Pf2-HA_OE* strain).

582

583   **5.   Acknowledgements**

27

6. References

597 1. McDonald MC, Solomon PS. 2018. Just the surface: advances in the discovery and

598 characterization of necrotrophic wheat effectors. Current Opinion in Microbiology

599 46:14–18.

600 2. Kanyuka K, Igna AA, Solomon PS, Oliver RP. 2022. The rise of necrotrophic effectors.

601 New Phytologist 233:11–14.

602 3. Friesen TL, Stukenbrock EH, Liu Z, Meinhardt S, Ling H, Faris JD, Rasmussen JB,

603 Solomon PS, McDonald BA, Oliver RP. 2006. Emergence of a new disease as a result

604 of interspecific virulence gene transfer. 8. Nature Genetics 38:953–956.

605 4. Liu Z, Faris JD, Oliver RP, Tan K-C, Solomon PS, McDonald MC, McDonald BA, Nunez

606 A, Lu S, Rasmussen JB, Friesen TL. 2009. SnTox3 acts in effector triggered

607 susceptibility to induce disease on wheat carrying the *Snn3* gene. PLOS Pathogens

608 5:e1000581.

609 5. Liu Z, Zhang Z, Faris JD, Oliver RP, Syme R, McDonald MC, McDonald BA, Solomon

610 PS, Lu S, Shelver WL, Xu S, Friesen TL. 2012. The cysteine rich necrotrophic effector

611 SnTox1 produced by *Stagonospora nodorum* triggers susceptibility of wheat lines

612 harboring *Snn1*. PLOS Pathogens 8:e1002467.

613 6. Kariyawasam GK, Richards JK, Wyatt NA, Running KLD, Xu SS, Liu Z, Borowicz P,

614 Faris JD, Friesen TL. 2022. The *Parastagonospora nodorum* necrotrophic effector

615 SnTox5 targets the wheat gene Snn5 and facilitates entry into the leaf mesophyll. New

616 Phytologist 233:409–426.

617 7. Richards JK, Kariyawasam GK, Seneviratne S, Wyatt NA, Xu SS, Liu Z, Faris JD,

618 Friesen TL. 2022. A triple threat: the *Parastagonospora nodorum* SnTox267 effector

619 exploits three distinct host genetic factors to cause disease in wheat. New Phytologist

620 233:427–442.

621   8.   Phan HTT, Rybak K, Furuki E, Breen S, Solomon PS, Oliver RP, Tan K-C. 2016.

622   Differential effector gene expression underpins epistasis in a plant fungal disease. The

623   Plant J 87:343–354.

624   9.   Peters-Haugrud AR, Zhang Z, Richards JK, Friesen TL, Faris JD. 2019. Genetics of

625   variable disease expression conferred by inverse gene-for-gene interactions in the

626   wheat-*Parastagonospora nodorum* pathosystem. Plant Physiology 180:420–434.

627   10.   John E, Jacques S, Phan HTT, Liu L, Pereira D, Croll D, Singh KB, Oliver RP, Tan K-C.

628   2022. Variability in an effector gene promoter of a necrotrophic fungal pathogen

629   dictates epistasis and effector-triggered susceptibility in wheat. PLOS Pathogens

630   18:e1010149.

631   11.   Cho Y, Ohm RA, Grigoriev IV, Srivastava A. 2013. Fungal-specific transcription factor

632   *AbPf2* activates pathogenicity in *Alternaria brassicicola*. The Plant J 75:498–514.

633   12.   Rybak K, See PT, Phan HTT, Syme RA, Moffat CS, Oliver RP, Tan K-C. 2017. A

634   functionally conserved Zn2Cys6 binuclear cluster transcription factor class regulates

635   necrotrophic effector gene expression and host-specific virulence of two major

636   Pleosporales fungal pathogens of wheat. Mol Plant Pathol 18:420–434.

637   13.   Jones DAB, John E, Rybak K, Phan HTT, Singh KB, Lin S-Y, Solomon PS, Oliver RP,

638   Tan K-C. 2019. A specific fungal transcription factor controls effector gene expression

639   and orchestrates the establishment of the necrotrophic pathogen lifestyle on wheat. 1.

640   Sci Rep 9:1–13.

641   14.   Clairet C, Gay EJ, Porquier A, Blaise F, Marais CL, Balesdent M-H, Rouxel T, Soyer

642   JL, Fudal I. 2021. Regulation of effector gene expression as concerted waves in

643   *Leptosphaeria maculans*: a two-players game. BioRxiv 2021.12.15.472773.

644   15.   John E, Singh KB, Oliver RP, Tan K-C. 2021. Transcription factor lineages in plant-

645   pathogenic fungi, connecting diversity with fungal virulence. Fungal Genetics and

646   Biology In press.

647   16.   Chung H, Choi J, Park S-Y, Jeon J, Lee Y-H. 2013. Two conidiation-related

648   Zn(II)2Cys6 transcription factor genes in the rice blast fungus. Fungal Genet Biol

649   61:133–141.

650   17.   Oh M, Son H, Choi GJ, Lee C, Kim J-C, Kim H, Lee Y-W. 2016. Transcription factor

651   ART1 mediates starch hydrolysis and mycotoxin production in *Fusarium graminearum*

652   and *F. verticillioides*. Mol Plant Pathol 17:755–768.

653   18.   Habig M, Bahena-Garrido SM, Barkmann F, Haueisen J, Stukenbrock EH. 2020. The

654   transcription factor Zt107320 affects the dimorphic switch, growth and virulence of the

655   fungal wheat pathogen *Zymoseptoria tritici*. Mol Plant Pathol 21:124–138.

656   19.   Han JW, Kim DY, Lee YJ, Choi YR, Kim B, Choi GJ, Han S-W, Kim H. 2020.

657   Transcription factor PdeR is involved in fungal development, metabolic change, and

658   pathogenesis of gray mold *Botrytis cinerea*. J Agric Food Chem 68:9171–9179.

659   20.   Nitta M, Furukawa T, Shida Y, Mori K, Kuhara S, Morikawa Y, Ogasawara W. 2012. A

660   new Zn(II)2Cys6-type transcription factor BglR regulates β-glucosidase expression in

661   *Trichoderma reesei*. Fungal Genet Biol 49:388–397.

662   21.   Xiong Y, Wu VW, Lubbe A, Qin L, Deng S, Kennedy M, Bauer D, Singan VR, Barry K,

663   Northen TR, Grigoriev IV, Glass NL. 2017. A fungal transcription factor essential for

664   starch degradation affects integration of carbon and nitrogen metabolism. PLOS

665   Genetics 13:e1006737.

666   22.   Wu VW, Thieme N, Huberman LB, Dietschmann A, Kowbel DJ, Lee J, Calhoun S,

667   Singan VR, Lipzen A, Xiong Y, Monti R, Blow MJ, O'Malley RC, Grigoriev IV, Benz JP,

668   Glass NL. 2020. The regulatory and transcriptional landscape associated with carbon

669   utilization in a filamentous fungus. PNAS 117:6003–6013.

670 23. Gabriel R, Thieme N, Liu Q, Li F, Meyer LT, Harth S, Jecmenica M, Ramamurthy M,

671   Gorman J, Simmons BA, McCluskey K, Baker SE, Tian C, Schuerg T, Singer SW,

672   Fleißner A, Benz JP. 2021. The F-box protein gene exo-1 is a target for reverse

673   engineering enzyme hypersecretion in filamentous fungi. Proc Natl Acad Sci U S A

674   118:e2025689118.

675 24. Li J, Liu Q, Li J, Lin L, Li X, Zhang Y, Tian C. 2021. RCO-3 and COL-26 form an

676   external-to-internal module that regulates the dual-affinity glucose transport system in

677   *Neurospora crassa*. Biotechnology for Biofuels 14:33.

678 25. Hane JK, Paxman J, Jones DAB, Oliver RP, de Wit P. 2020. "CATAStrophy," a

679   genome-informed trophic classification of filamentous plant pathogens – how many

680   different types of filamentous plant pathogens are there? Front Microbiol 10.

681 26. MacPherson S, Larochelle M, Turcotte B. 2006. A fungal family of transcriptional

682   regulators: the zinc cluster proteins. Microbiol Mol Biol Rev 70:583–604.

683 27. Schubert S, Popp C, Rogers PD, Morschhäuser J. 2011. Functional dissection of a

684   *Candida albicans* zinc cluster transcription factor, the multidrug resistance regulator

685   Mrr1. Eukaryotic Cell 10:1110–1121.

686 28. Erdős G, Dosztányi Z. 2020. Analyzing Protein Disorder with IUPred2A. Current

687   Protocols in Bioinformatics 70:e99.

688 29. Zhang Y, Liu T, Meyer CA, Eeckhoute J, Johnson DS, Bernstein BE, Nusbaum C,

689   Myers RM, Brown M, Li W, Liu XS. 2008. Model-based Analysis of ChIP-Seq (MACS).

690   Genome Biology 9:R137.

691   30.   Ipcho SVS, Hane JK, Antoni EA, Ahren D, Henrissat B, Friesen TL, Solomon PS, Oliver

692   RP. 2012. Transcriptome analysis of *Stagonospora nodorum*: gene models, effectors,

693   metabolism and pantothenate dispensability. Mol Plant Pathol 13:531–545.

694   31.   Siggers T, Duyzend MH, Reddy J, Khan S, Bulyk ML. 2011. Non-DNA-binding

695   cofactors enhance DNA-binding specificity of a transcriptional regulatory complex. Mol

696   Syst Biol 7:555.

697   32.   Kojima T, Kunitake E, Ihara K, Kobayashi T, Nakano H. 2016. A robust analytical

698   pipeline for genome-wide identification of the genes regulated by a transcription factor:

699   combinatorial analysis performed using gSELEX-Seq and RNA-Seq. PLOS ONE

700   11:e0159011.

701   33.   Zhao C, Waalwijk C, de Wit PJGM, van der Lee T, Tang D. 2011. EBR1, a novel

702   Zn(2)Cys(6) transcription factor, affects virulence and apical dominance of the hyphal

703   tip in *Fusarium graminearum*. Mol Plant Microbe Interact 24:1407–1418.

704   34.   Jonkers W, Xayamongkhon H, Haas M, Olivain C, van der Does HC, Broz K, Rep M,

705   Alabouvette C, Steinberg C, Kistler HC. 2014. *EBR1* genomic expansion and its role in

706   virulence of *Fusarium* species. Environ Microbiol 16:1982–2003.

707   35.   Adnan M, Zheng W, Islam W, Arif M, Abubakar YS, Wang Z, Lu G. 2017. Carbon

708   catabolite repression in filamentous fungi. Int J Mol Sci 19:48.

709   36.   John E, Singh KB, Oliver RP, Tan K-C. 2021. Transcription factor control of virulence in

710   phytopathogenic fungi. Mol Plant Pathol 22:858–881.

711   37.   Gomi K. 2019. Regulatory mechanisms for amylolytic gene expression in the koji mold

712   *Aspergillus oryzae*. Bioscience, Biotechnology, and Biochemistry 83:1385–1401.

713   38. Wang P, Kojima T, Kobayashi T, Nakano H. 2012. Comprehensive analysis of the
714   DNA-binding specificity of an *Aspergillus nidulans* transcription factor, AmyR, using a
715   bead display system. Biosci Biotechnol Biochem 76:1128–1134.

716   39. Tani S, Katsuyama Y, Hayashi T, Suzuki H, Kato M, Gomi K, Kobayashi T, Tsukagoshi
717   N. 2001. Characterization of the *amyR* gene encoding a transcriptional activator for the
718   amylase genes in *Aspergillus nidulans*. Curr Genet 39:10–15.

719   40. Nakamura T, Maeda Y, Tanque N, Makita T, Kato M, Kobayashi T. 2006. Expression
720   profile of amylolytic genes in *Aspergillus nidulans*. Bioscience, Biotechnology, and
721   Biochemistry 70:2363–2370.

722   41. Marín-Menguiano M, Moreno-Sánchez I, Barrales RR, Fernández-Álvarez A, Ibeas JI.
723   2019. N-glycosylation of the protein disulfide isomerase Pdi1 ensures full *Ustilago*
724   *maydis* virulence. PLOS Pathogens 15:e1007687.

725   42. Lin S-Y, Chooi Y-H, Solomon PS. 2018. The global regulator of pathogenesis PnCon7
726   positively regulates *Tox3* effector gene expression through direct interaction in the
727   wheat pathogen *Parastagonospora nodorum*. Molecular Microbiology 109:78–90.

728   43. Craig JP, Coradetti ST, Starr TL, Glass NL. 2015. Direct target network of the
729   *Neurospora crassa* plant cell wall deconstruction regulators CLR-1, CLR-2, and XLR-1.
730   mBio 6.

731   44. IpCho SVS, Tan K-C, Koh G, Gummer J, Oliver RP, Trengove RD, Solomon PS. 2010.
732   The transcription factor StuA regulates central carbon metabolism, mycotoxin
733   production, and effector gene expression in the wheat pathogen *Stagonospora*
734   *nodorum*. Eukaryotic Cell 9:1100–1108.

735   45. Chooi Y-H, Zhang G, Hu J, Muria-Gonzalez MJ, Tran PN, Pettitt A, Maier AG, Barrow
736   RA, Solomon PS. 2017. Functional genomics-guided discovery of a light-activated

737   phytotoxin in the wheat pathogen *Parastagonospora nodorum* via pathway activation.

738   Environ Microbiol 19:1975–1986.

739   46. Slattery M, Zhou T, Yang L, Dantas Machado AC, Gordân R, Rohs R. 2014. Absence

740   of a simple code: how transcription factors read the genome. Trends in Biochemical

741   Sciences 39:381–399.

742   47. Reiter F, Wienerroither S, Stark A. 2017. Combinatorial function of transcription factors

743   and cofactors. Current Opinion in Genetics & Development 43:73–81.

744   48. Carey MF, Peterson CL, Smale ST. 2012. Confirming the Functional Importance of a

745   Protein–DNA Interaction. Cold Spring Harb Protoc 2012:pdb.top070060.

746   49. Spivakov M. 2014. Spurious transcription factor binding: non-functional or genetically

747   redundant? Bioessays 36:798–806.

748   50. Osterwalder M, Barozzi I, Tissières V, Fukuda-Yuzawa Y, Mannion BJ, Afzal SY, Lee

749   EA, Zhu Y, Plajzer-Frick I, Pickle CS, Kato M, Garvin TH, Pham QT, Harrington AN,

750   Akiyama JA, Afzal V, Lopez-Rios J, Dickel DE, Visel A, Pennacchio LA. 2018.

751   Enhancer redundancy allows for phenotypic robustness in mammalian development.

752   Nature 554:239–243.

753   51. Soyer JL, Ghalid ME, Glaser N, Ollivier B, Linglin J, Grandaubert J, Balesdent M-H,

754   Connolly LR, Freitag M, Rouxel T, Fudal I. 2014. Epigenetic control of effector gene

755   expression in the plant pathogenic fungus *Leptosphaeria maculans*. PLOS Genetics

756   10:e1004227.

757   52. Soyer JL, Möller M, Schotanus K, Connolly LR, Galazka JM, Freitag M, Stukenbrock

758   EH. 2015. Chromatin analyses of *Zymoseptoria tritici*: methods for chromatin

759   immunoprecipitation followed by high-throughput sequencing (ChIP-seq). Fungal Genet

760   Biol 79:63–70.

761   53.   Bewick AJ, Hofmeister BT, Powers RA, Mondo SJ, Grigoriev IV, James TY, Stajich JE,

762   Schmitz RJ. 2019. Diversity of cytosine methylation across the fungal tree of life. 3.

763   Nature Ecology & Evolution 3:479–490.

764   54.   Syme RA, Tan K-C, Hane JK, Dodhia K, Stoll T, Hastie M, Furuki E, Ellwood SR,

765   Williams AH, Tan Y-F, Testa AC, Gorman JJ, Oliver RP. 2016. Comprehensive

766   annotation of the *Parastagonospora nodorum* reference genome using next-generation

767   genomics, transcriptomics and proteogenomics. PLOS ONE 11:e0147221.

768   55.   Blum M, Chang H-Y, Chuguransky S, Grego T, Kandasaamy S, Mitchell A, Nuka G,

769   Paysan-Lafosse T, Qureshi M, Raj S, Richardson L, Salazar GA, Williams L, Bork P,

770   Bridge A, Gough J, Haft DH, Letunic I, Marchler-Bauer A, Mi H, Natale DA, Necci M,

771   Orengo CA, Pandurangan AP, Rivoire C, Sigrist CJA, Sillitoe I, Thanki N, Thomas PD,

772   Tosatto SCE, Wu CH, Bateman A, Finn RD. 2020. The InterPro protein families and

773   domains database: 20 years on. Nucleic Acids Res

774   https://doi.org/10.1093/nar/gkaa977.

775   56.   Nguyen Ba AN, Pogoutse A, Provart N, Moses AM. 2009. NLStradamus: a simple

776   Hidden Markov Model for nuclear localization signal prediction. BMC Bioinformatics

777   10:202.

778   57.   Andrews S. 2010. Babraham Bioinformatics - FastQC a quality control tool for high

779   throughput sequence data. https://www.bioinformatics.babraham.ac.uk/projects/fastqc/.

780   Retrieved 26 April 2021.

781   58.   Martin M. 2011. Cutadapt removes adapter sequences from high-throughput

782   sequencing reads. 1. EMBnet.journal 17:10–12.

783   59.   Bushnell B. 2016. BBMap. SourceForge. https://sourceforge.net/projects/bbmap/.

784   Retrieved 26 April 2021.

785   60.   Li H. 2013. Aligning sequence reads, clone sequences and assembly contigs with

786   BWA-MEM. arXiv:13033997 [q-bio].

787   61.   Li H, Handsaker B, Wysoker A, Fennell T, Ruan J, Homer N, Marth G, Abecasis G,

788   Durbin R, 1000 Genome Project Data Processing Subgroup. 2009. The sequence

789   alignment/map format and SAMtools. Bioinformatics 25:2078–2079.

790   62.   Feng J, Liu T, Qin B, Zhang Y, Liu XS. 2012. Identifying ChIP-seq enrichment using

791   MACS. 9. Nat Protoc 7:1728–1740.

792   63.   Gaspar JM. 2018. Improved peak-calling with MACS2. bioRxiv 496521.

793   64.   Ramírez F, Ryan DP, Grüning B, Bhardwaj V, Kilpert F, Richter AS, Heyne S, Dündar

794   F, Manke T. 2016. deepTools2: a next generation web server for deep-sequencing data

795   analysis. Nucleic Acids Res 44:W160–W165.

796   65.   Shao Z, Zhang Y, Yuan G-C, Orkin SH, Waxman DJ. 2012. MAnorm: a robust model

797   for quantitative comparison of ChIP-Seq data sets. Genome Biology 13:R16.

798   66.   Bailey TL, Boden M, Buske FA, Frith M, Grant CE, Clementi L, Ren J, Li WW, Noble

799   WS. 2009. MEME SUITE: tools for motif discovery and searching. Nucleic Acids Res

800   37:W202-208.

801   67.   Bailey TL, Elkan C. 1994. Fitting a mixture model by expectation maximization to

802   discover motifs in biopolymers. Proc Int Conf Intell Syst Mol Biol 2:28–36.

803   68.   Bailey TL, Machanick P. 2012. Inferring direct DNA binding from ChIP-seq. Nucleic

804   Acids Res 40:e128–e128.

805   69.   Grant CE, Bailey TL, Noble WS. 2011. FIMO: scanning for occurrences of a given

806   motif. Bioinformatics 27:1017–1018.

807   70.   Armstrong RA. 2014. When to use the Bonferroni correction. Ophthalmic Physiol Opt

808   34:502–508.

809   71.   Yu G, Wang L-G, He Q-Y. 2015. ChIPseeker: an R/Bioconductor package for ChIP

810   peak annotation, comparison and visualization. Bioinformatics 31:2382–2383.

811   72.   Lin X, Tirichine L, Bowler C. 2012. Protocol: Chromatin immunoprecipitation (ChIP)

812   methodology to investigate histone modifications in two model diatom species. Plant

813   Methods 8:48.

814   73.   Bursteinas B, Britto R, Bely B, Auchincloss A, Rivoire C, Redaschi N, O'Donovan C,

815   Martin MJ. 2016. Minimizing proteome redundancy in the UniProt Knowledgebase.

816   Database : J Biol Databases Curation 2016.

817   74.   Yu G, Wang L-G, Han Y, He Q-Y. 2012. clusterProfiler: an R package for comparing

818   biological themes among gene clusters. OMICS: A Journal of Integrative Biology

819   16:284–287.

820

821

822   **7.   Tables**

823   **Table 1.** Rationale for the investigation of novel transcription factors (TFs) in this study

TF investigated	Involvement	Virulence-associated orthologues [A]
PnPro1 (SNOG_3490)	Directly-positively regulated by PnPf2	*AbPro1* (*Ab*), *MoPRO1* (*Mo*), *GzZC232* (*Fg*), *UvPro1* (*Uv*)
PnAda1 (SNOG_04486)	Directly-positively regulated by PnPf2	*GzbZIP001* (*Fg*), *FpAda1* (*Fp*)
SNOG_08237	Directly-positively regulated by PnPf2	*CoHox1* (*Co*)
SNOG_08565	Shared ancestral lineage with PnPf2 orthologues	-
PnEbr1 (SNOG_03067)	Co-expressed with *PnPf2*, *ToxA*, *Tox1* and *Tox3* during infection	*EBR1* (*Fg*), *EBR1* (*Fo*), *MoCod2* and *Cnf2* (*Mo*)
PnCreA (SNOG_13619)	Enriched CreA-binding motif (22) in PnPf2-regulated gene promoters	*CreA* (*Af*), *Cre1* (*Fo*), *CreA* (*Pe*)

824   [A] Putative orthologues were inferred by cross-referencing a previous TF-orthology analysis
825   and literature review (15, 36). Abbreviations: *Ab; Alternaria brassicicola*, *Af; Aspergillus*
826   *flavus*, *Co; Colletotrichum orbiculare, Fg; Fusarium graminearum, Fo; Fusarium oxysporum,*
827   *Fp; Fusarium pseudograminearum, Mo; Magnaporthe oryzae*, *Pe; Penicillium expansum*.
828

829

830   **Table 2.** Overview of the strains referenced in this study [A]

| Strain ID	Description [B]
SN15	Wildtype *P. nodorum* reference isolate
pf2ko	Original *PnPf2* deletion mutant (12, 13)
pf2_KO	*PnPf2* deletion mutant to facilitate targeted complementation
Pf2_OE	*PnPf2* overexpression (*pGpdA* promoter)
Pf2-GFP	*PnPf2* with *GFP* tag, native promoter
Pf2-GFP_OE	*PnPf2* with *GFP* tag, overexpression promoter
Pf2-HA	*PnPf2* with 3x*HA* tag, native promoter
Pf2-HA_OE	*PnPf2* with 3x*HA* tag, overexpression promoter
pf2-HA_KO	*PnPf2* coding sequence replaced with 3x*HA* tag
CreA_OE	*PnCreA* overexpression (*pGpdA* promoter)
creA_KO	*PnCreA* deletion mutant
CreA_Ec	*PnCreA* ectopically-integrated construct
SN15-*GFP*	SN15 constitutively expressing *GFP*
pTef1-dTom	SN15 constitutively expressing *dTomato* (defined locus)
p15417_M1M2	SN15 expressing *dTomato* (defined locus) SNOG_15417 promoter, no mutations
p15417_m1M2	SN15 expressing *dTomato* (defined locus) SNOG_15417 promoter, M1 mutated
p15417_M1m2	SN15 expressing *dTomato* (defined locus) SNOG_15417 promoter, M2 mutated
p15417_m1m2	SN15 expressing *dTomato* (defined locus) SNOG_15417 promoter, M1+2 mutated
pro1_KO	*PnPro1* deletion mutant
Pro1_comp	*PnPro1* complemented in *pro1_KO* background
ada1_KO	*PnAda1* deletion mutant
Ada1_comp	*PnAda1* complemented in *ada1_KO* background
08237_KO	SNOG_08237 deletion mutant
08237_comp	SNOG_08237 complemented in *08237_KO* background
08565_KO	SNOG_08565 deletion mutant
08565_comp	SNOG_08565 complemented in *08565_KO* background
ebr1_KO	*PnEbr1* deletion mutant
Ebr1_Ec	*PnEbr1* ectopically-integrated construct

831   [A] Strains are listed in corresponding order to the detailed description of their generation in
832   Text S3.

833   [B] Abbreviations: GFP – Green fluorescent protein, HA – Haemagglutinin, M1 – Motif1, M2 –
834   Motif 2.

835

8. Figures

837

838
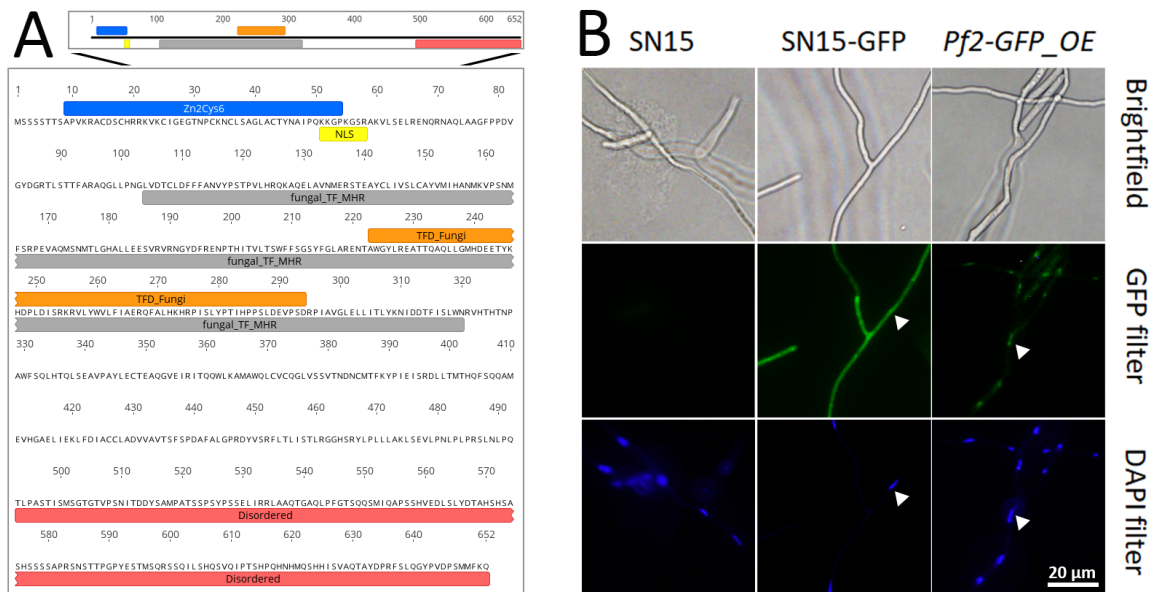
Fig. 1 PnPf2 domain analysis and cellular localisation. A) Predicted domains and features identified in the 652 amino acid PnPf2 protein sequence typical of a Zn_2Cys_6 transcription factor (TF). The region corresponding to the N-terminal Zn_2Cys_6 DNA binding domain (Zn_2Cys_6 - Interpro IPR001138) is depicted in blue and the nuclear localisation signal (NLS) is in yellow. The fungal transcription factor domain (TFD_fungi - Interpro IPR007219) corresponds to orange within the 'middle homology region' (fungal_TF_MHR - Conserved Domain Database CD12148) depicted in grey. A C-terminal disordered protein region lacking secondary structure was identified that corresponds to the red bar. B) Epifluorescence microscopy depicting nuclear localisation of the GFP-tagged PnPf2 translational fusion specific to the *Pf2-GFP_OE* overexpression strain, in contrast to the wildtype (SN15) and the positive control strain expressing cytoplasmic GFP (SN15-*GFP*). Arrows indicate the corresponding locations of fungal nuclei under the respective filters determined by DAPI staining of a germinated pycnidiospore. A fluorescence signal was not detected in the *Pf2-GFP*

853   strain, where expression was driven by the native *PnPf2* promoter, indicating PnPf2

854   accumulates at relatively low abundance.

855

856

857

41
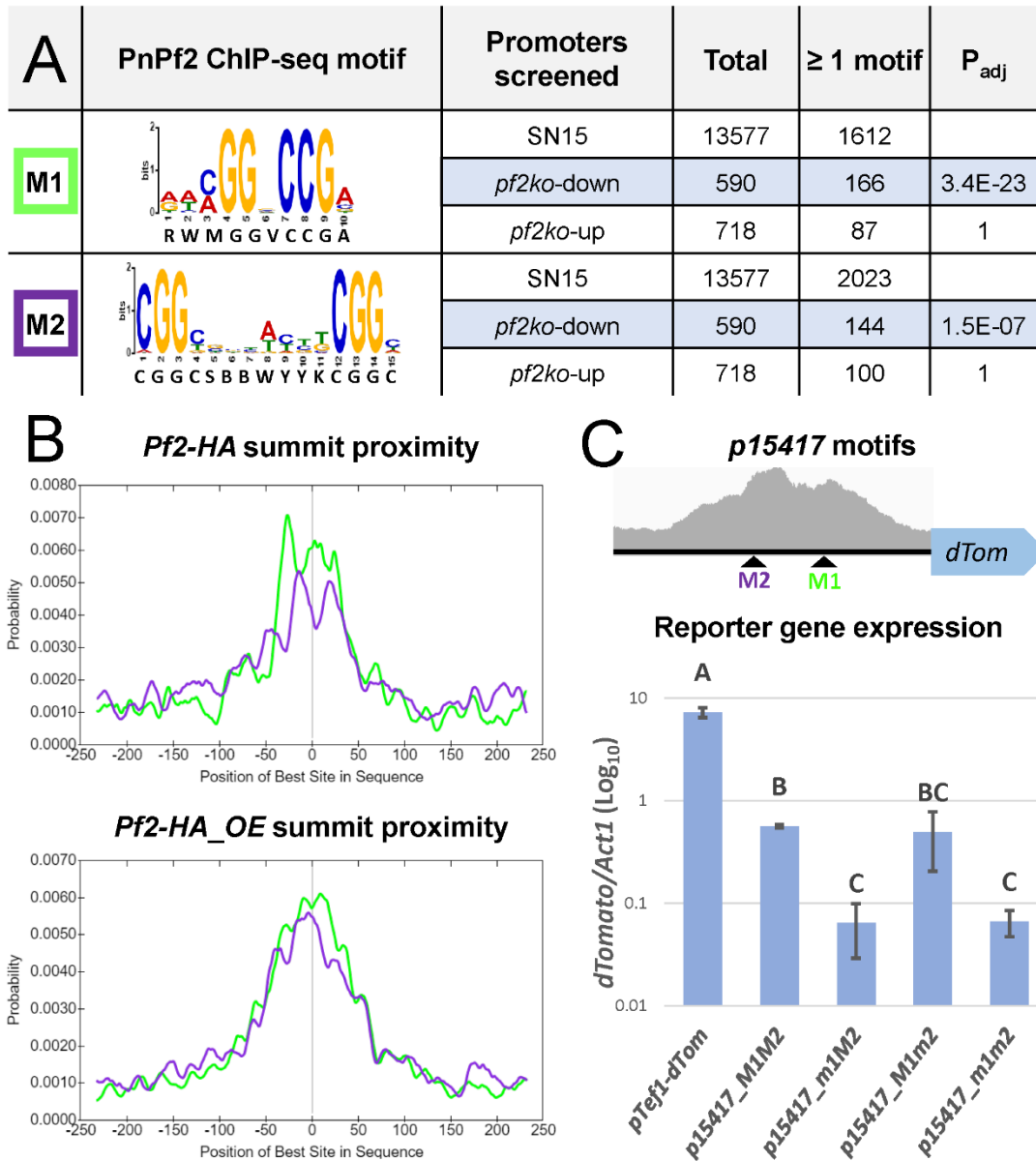
Fig. 2 Identification of PnPf2 regulatory element motifs. **A)** The M1 motif (5'-RWMGGVCCGA-3') and M2 motif (5'-CGGCSBBWYYKCGGC-3') were modelled from the merged set of *Pf2-HA* and *Pf2-HA_OE* sample ChIP-seq peak regions. Their detection (≥ 1 occurrence) in the promoters of PnPf2 positively (*pf2ko*-down) or negatively (*pf2ko*-up) regulated gene promoters (13) are indicated relative to all SN15 promoters. The P_{adj} value reflects the test for significant enrichment (Fisher's test with Bonferroni $P_{adj} < 0.01$), where both motifs were enriched in the *pf2ko*-down genes relative to SN15. **B)** The position of motif occurrences relative to ChIP-seq summits,

867 demonstrating their higher likelihood at close proximity to the best estimate of PnPf2-

868 DNA binding loci. **C)** Gene expression analysis assessing the effect of M1 and M2

869 motif mutation in *P. nodorum in situ*. The motif loci within a ChIP-seq peak in the

870 SNOG_15417 gene promoter region (*p15417*) are depicted. The *dTomato* reporter

871 gene was fused to a constitutive promoter control (*pTef1-dTom*) or the SNOG_15417

872 gene promoter (*p15417_M1M2*) in the *P. nodorum* background. The motifs were also

873 mutated through substitution of the respective 'CGG' triplets, alone or in combination

874 (*p15417_m1M2, p15417_M1m2* and *p15417_m1m2*). The strains *p15417_m1M2* and

875 *p15417_m1m2* where M1 had been mutated exhibited significantly reduced

876 expression relative to the non-mutated promoter in *p15417_M1M2*. This suggested

877 PnPf2 regulatory activity had been impaired following M1 mutation but not M2 mutation

878 in *p15417*. Letters indicate statistically distinct groupings by ANOVA with Tukey's-HSD

879 (P<0.05).

880
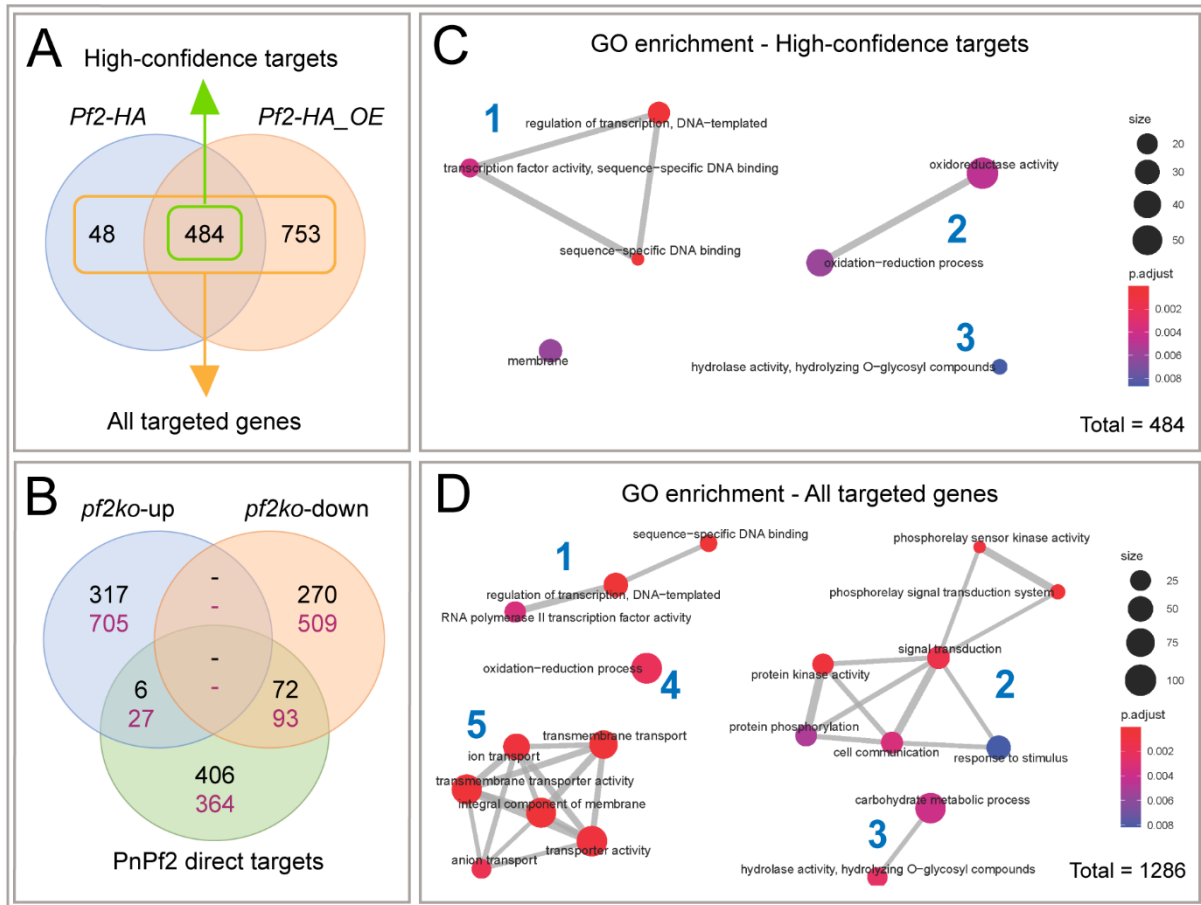
Fig. 3 Gene expression and gene-ontology (GO) analysis of PnPf2 direct targets. **A)** Overview of the genes targeted by PnPf2 in their promoter region based on the respective *Pf2-HA* and *Pf2-HA_OE* ChIP-seq datasets. There were 484 genes considered high-confidence PnPf2 targets among the 1286 putative targets from either construct. **B)** The high-confidence targets in comparison with their expression pattern in the *pf2ko* deletion mutant. Black numbers correspond to the *in vitro* growth conditions replicated for ChIP-seq sample preparation while purple numbers also encompass differentially expressed genes during early infection. The greater overlap with PnPf2 positively-regulated (*pf2ko*-down - 72 genes) than repressed (*pf2ko*-up - 6 genes) suggested PnPf2 predominantly functions as a positive regulator of gene expression. **C-D)** A summary of significantly-enriched GO terms among PnPf2-targeted genes. The high-confidence (*Pf2-HA* and *Pf2-HA_OE*) and total identified

894   targets (*Pf2-HA* or *Pf2-HA_OE*) are both displayed for comparison. Bubble sizes are

895   proportionate to gene counts, colours to the enrichment test *P* values and the lines

896   between bubbles to the total shared terms. Numbers in blue indicate connected gene

897   networks representing transcription factors [number 1], redox molecules [2],

898   carbohydrate-active enzymes [3], cell-signalling molecules [4], and trans-membrane

899   transporters [5].
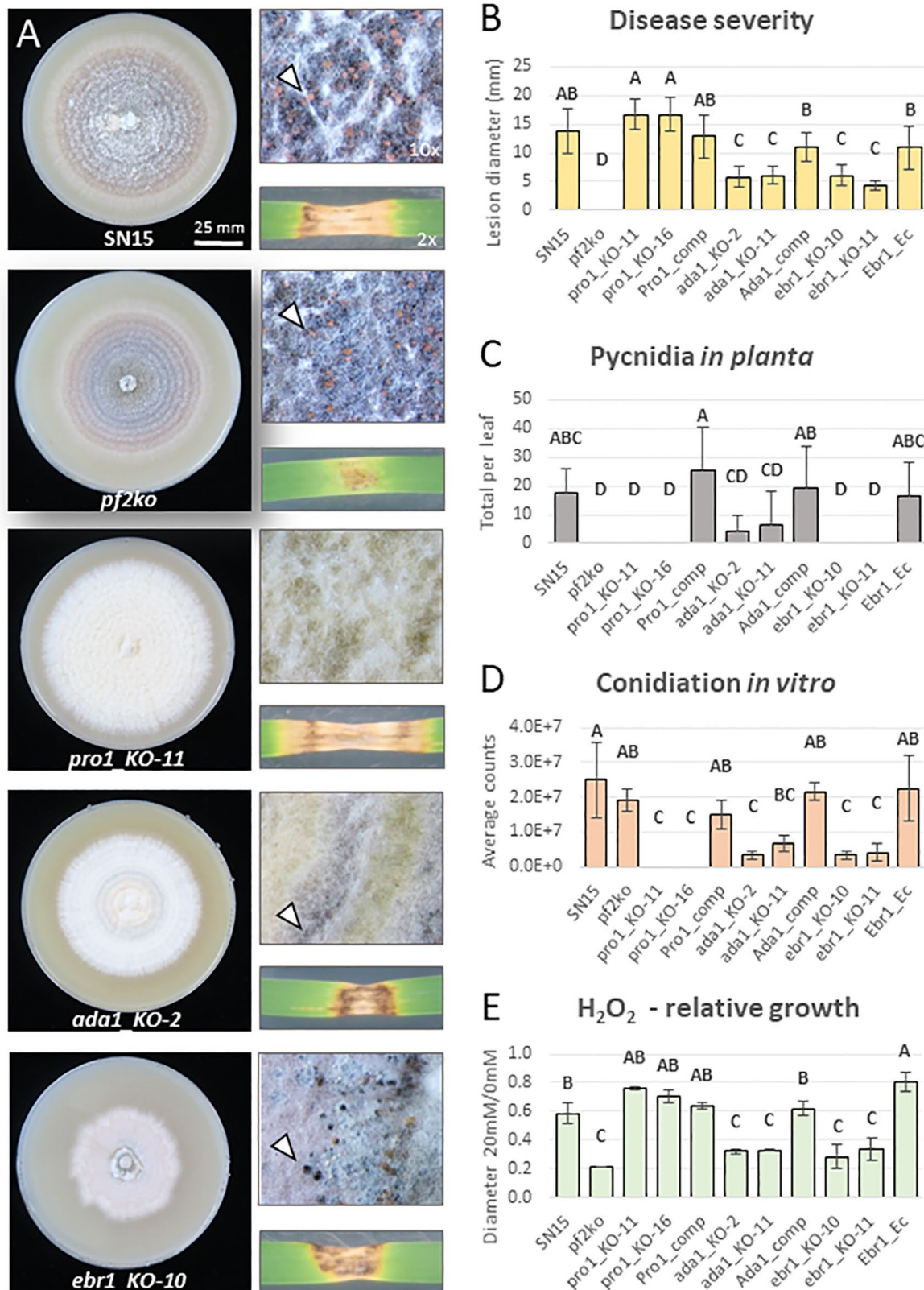
902   **Fig. 4** Phenotypic assessment of transcription factor (TF) gene deletion mutants. **A)**

903   Representative images after 12 days of growth on nutrient-rich agar (V8PDA) and

904   infection on detached wheat leaves (cv. Halberd). Arrows demonstrate pycnidia if they

905   were detected in the respective mutants. **B)** Average lesion sizes representing disease

906   severity. **C)** Pycnidia counts, a measure of pathogenic fitness following the infection.

907   **D)** Average conidial (pycnidiospore) counts on V8PDA. **E)** Growth inhibition on 20mM

908   H_2O_2 relative to 0mM on minimal medium agar. Letters indicate statistically distinct

909   groupings by ANOVA with Tukey's-HSD ($P<0.05$).

910
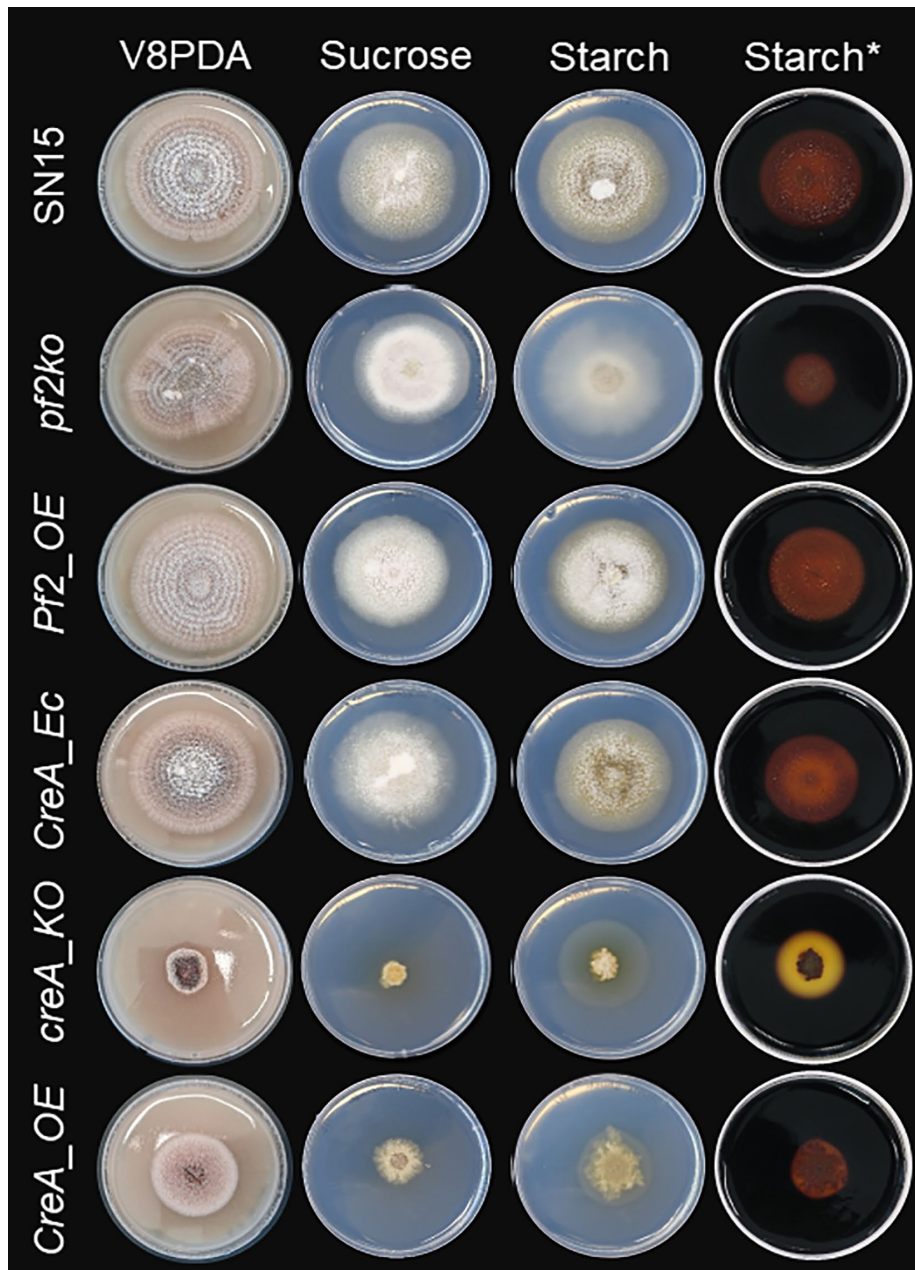
Fig. 5 Assessment of *PnPf2* and *PnCreA* mutant growth on different substrates. Images following 12 days of growth on nutrient-rich V8PDA and minimal-medium agar with a primary (sucrose) or secondary (starch) carbon source. Wildtype SN15 and the respective mutants are listed on each row. The capacity to fully utilise starch was enhanced in the *creA_KO* mutant despite growth defects, suggesting impaired carbon-catabolite repression. Starch utilisation was moderately reduced in the *pf2ko* mutant. *Post-stained with Lugol's iodine to assist visualisation of starch hydrolysis.
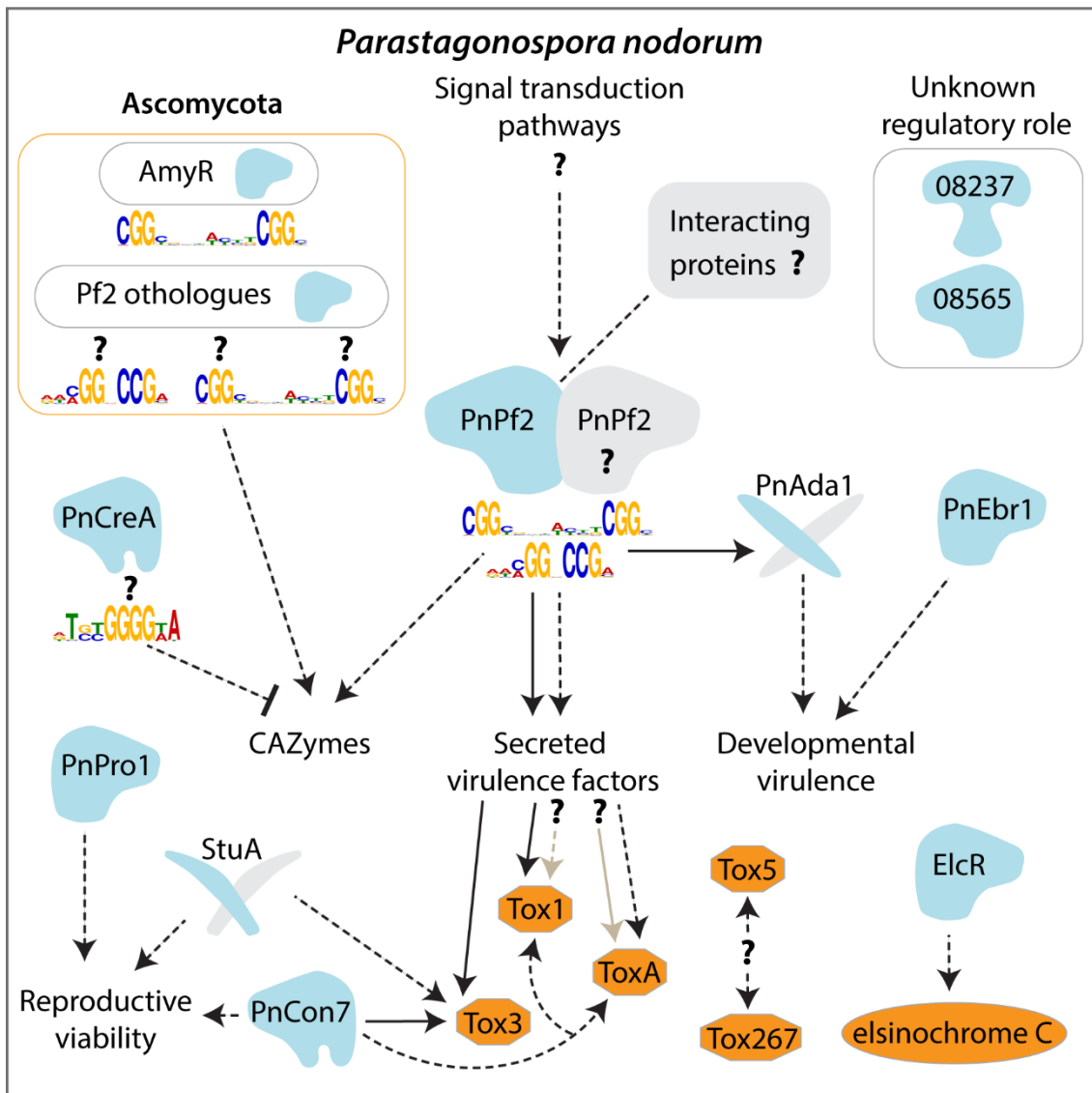
Fig. 6 The proposed model of the PnPf2-centred regulatory network in the virulence of *P. nodorum*. The Pf2 taxonomic orthologues and AmyR regulators in the Ascomycota fungi (discussed in the main text) are presented for context regarding the two PnPf2 regulatory motifs described in this study. Transcription factors (TFs) and virulence factors that are cloned and characterised in *P. nodorum* are depicted (blue and orange shapes respectively; grey shapes indicate putative interacting proteins). Dashed arrows show where gene regulation occurs and solid arrows represent direct regulation. Question marks are presented where evidence is tentative and requires validation. PnPf2 controls the expression of key virulence

930   factors. The effector *Tox3* is directly regulated and *ToxA*, based on promoter-motif

931   and gene expression data, is likely a direct target during plant infection. PnPf2 also

932   directly targets the *Tox1* promoter as a possible enhancer while regulators of *Tox267*

933   and *Tox5* require investigation. Carbohydrate-active enzymes (CAZymes) are also

934   regulated by PnPf2, with a subset putatively repressed by PnCreA for which no

935   distinct role in virulence has been established. Developmental virulence, such as

936   oxidative stress tolerance and hyphal growth, were processes attributed in this study

937   to the PnPf2 targets PnAda1 and PnEbr1. PnPro1 and StuA (44) are essential for

938   reproduction by sporulation, while no distinct role was identified for the putative TFs

939   encoded by SNOG_08237 and SNOG_08565. Elsewhere, PnCon7 has been

940   reported to regulate effector expression but is an essential viability factor, while

941   production of a phytotoxic metabolite elsinochrome C is controlled by the pathway-

942   specific ElcR gene-cluster TF (45, 42).

943

944

945   **9.   Supplemental item legends**

946   **Text S1** Chromatin immunoprecipitation (ChIP) strain assessment and

947   overview of ChIP-seq/ChIP-qPCR.

948   **Text S2** Supplemental transcription factor mutant phenotype assessment.

949   **Text S3** Supplemental materials and methods.

950   **Fig. S1** A depiction of the PnPf2 targeting of characterised effector genes in *P.*

951   *nodorum* SN15. The *Pf2-HA* and *Pf2-HA_OE* ChIP-seq read peaks are presented at

952   the *Tox3*, *Tox1*, *ToxA* and *Tox267* promoters. Peak summits were evident in the *Tox3*

953   and *Tox1* promoters. Red dots represent instances of the M1 motif (5'-

954   RWMGGVCCGA-3') and blue dots M2 (5'-CGGCSBBWYYKCGGC-3').

955   **Fig. S2** A heatmap depiction of *Parastagonospora nodorum* SN15 hierarchical

956   cluster analysis. Clustering was based on microarray gene-expression data during

957   infection (*in planta*) or axenic (*in vitro*) growth obtained from a previous study (30).

958   Clusters were cut into the 10 most distant clusters to identify genes co-expressed with

959   *PnPf2*, *ToxA*, *Tox1* and *Tox3*, which included the Zn_2Cys_6 transcription factor *PnEbr1*

960   (SNOG_03037) therefore investigated in this study.

961   **File S1** A spreadsheet detailing the genomic coordinates for ChIP-seq peak

962   regions [columns A-D], the respective summit loci [E], the pileup height of the mapped

963   reads [F] and the summit -Log_{10}(Q-values) representing the difference of ChIP reads

964   relative to the input control sample [G]. The *Pf2-HA* strain encompasses columns A-G

965   and the *Pf2-HA_OE* strain encompasses column H-N. Also included are the genomic

966   coordinates for the peak regions obtained by merging the overlapping regions from

967   the *Pf2-HA* and *Pf2-HA_OE* samples using MAnorm (65) [O-S].

968   **File S2** A spreadsheet of PnPf2 regulation data across the *P*. *nodorum* SN15

969   genome for the respective annotated genes [column A]. Listed are whether ChIP-seq

970   promoter summits were called from the *Pf2-HA* and *Pf2-HA_OE* samples [B-C],

971   whether the enriched PnPf2 target motifs [D-E] or the putative PnCreA motif [G] were

972   present in the gene promoter regions, and whether the gene was also down-regulated

973   in the *pf2ko* mutant [G]. Also listed are the functional annotations [G-M]; whether the

974   gene was classed as effector-like [H], a TF [I], the associated GO IDs/terms [J-K] and

975   Interpro domain information [L-M]. The final columns list the respective gene

976   expression data for *pf2ko* compared with SN15 either *in vitro* (*iv*) or *in planta* (*ip*) [13-

977   22]. *Information indicated was derived from Jones et al. (2019) for comparative

978   purposes.

979   **File S3** A spreadsheet compilation of the primers used in this study organised

980   by their general use [column 1] with the primer ID and sequence [2-3] and descriptions

981   for their use [4-5]. Highlighted in italics are restriction enzyme recognition sites, in bold

982   are overlapping regions used in cloning and in red are sites for incorporating single

983   nucleotide changes during cloning.

984

985